

Synthesis and photocatalytic activity studies of Silver-Nitrogen co-doped ZnO-Fe₂O₃ nanocomposites for the degradation of Methylene blue under UV-Visible region

Wondimagegn Kumala

Department of Chemistry, College of Natural and Computational Sciences, Mizan-Tepi University, Ethiopia.

Abstract: The binary systems of ZnO-Fe₂O₃ nanocomposites were synthesized by a precipitation method with aqueous solutions of Fe and Zn nitrate, whereas nitrogen-doped ZnO-Fe₂O₃, silver-doped ZnO-Fe₂O₃, and silver-nitrogen co-doped ZnO-Fe₂O₃ nanocomposite were prepared by solid-state reaction. The structure and bandgap of the composites were studied using X-ray diffraction (XRD) and UV-visible diffuse reflectance spectroscopy (UV-vis). An aqueous model pollutant Methylene blue (MB) dye solution was used to evaluate photocatalytic degradation activities of the nanocomposites under visible light irradiation. Doping photocatalyst significantly increased the effectiveness of the photocatalyst in reducing bandgap energy. So 2.05 eV is the lowest energy, which is for Ag/N co-doped ZnO-Fe₂O₃ photocatalysts. Results of the experiment that involved the photocatalysts revealed that Methylene blue degradations of 45.11%, 47%, 51%, and 64.5% in 180 min under light radiation using ZnO-Fe₂O₃, Ag-doped ZnO-Fe₂O₃, N-doped ZnO-Fe₂O₃, and Ag/N co-doped ZnO-Fe₂O₃, respectively. The doped photocatalysts were all superior to the undoped ZnO-Fe₂O₃. The efficiency of Ag/N co-doped ZnO-Fe₂O₃ photocatalysts was higher on the photodegradation of MB at optimum PH, the load of Methylene blue photocatalyst which is 78%.

Keywords: Nanocomposite; Binary system; doping, co-doping, and coupling; Photocatalysis.

1. Introduction

Currently, industrial effluents, agricultural runoff, and chemical spills are familiar sources for a variety of dyes that are being introduced into the water system. Among the causes of much concern to societies and regulation authorities around the world are their toxicity, stability to natural decomposition, and persistence in the environment ¹. Wastewater effluents from different industries such as textiles, rubber, paper, and plastics contain several kinds of synthetic dyestuffs. A minimal amount of dye in water is highly visible. The discharging of even a small amount of dye into the water can affect aquatic life and food webs due to the carcinogenic and mutagenic effects of synthetic dyes ¹. Photocatalytic technology has become a significant way of dominating environmental pollution. Heterogeneous photocatalysis has already been investigated and successfully applied to the degradation of different categories of organic compounds ².

The absorption of a photon initiates the photodecomposition of semiconductor with energy greater than or equal to the bandgap of semiconductor producing electron-hole pairs ³. It is important for prolonging electron-hole recombination before a designated chemical reaction

occurs on the semiconductor surface. Several semiconductor photocatalysts such as TiO₂, ZnO, WO₃, SnO₂, CdS, and ZnS ⁴ have been used for the treatment of wastewater pollutants under visible light irradiation. Among semiconductors, zinc oxide has attracted attention due to its environmental stability as compared to other metal oxides ⁵. Application of photocatalysis, especially using semiconductors such as ZnO, appears to be a more appealing approach than the conventional chemical oxidation methods for decomposition of toxic compounds to non-hazardous product ⁶. This is because semiconductors are: (i) inexpensive, (ii) non-toxic, (iii) having high surface area, (iv) having broad absorption spectra with high absorption coefficients, and (v) affording facility for the multi-electron transfer process. ZnO has been demonstrated as an improved photocatalyst as compared to commercialized TiO₂ based on its more significant initial rate of activities and higher absorption efficacy of solar radiations ⁷. However, ZnO has almost the same bandgap as TiO₂. Surface area and surface defects play an essential role in the photocatalytic activities of metal oxide. The photocatalytic activity of ZnO is restricted to the irradiation wavelengths in the UV region because of its wide bandgap of about 3.2 eV and low quantum efficiency ⁸. The wide bandgap and fast electrons

*Corresponding author: Wondimagegn Kumala

Email address: wondmes@yahoo.com

DOI: <http://dx.doi.org/10.13171/mjc107020071461wk>

Received April 28, 2020

Accepted June 1, 2020

Published July 23, 2020

recombination of ZnO constrains its application. This limitation has been improved by different strategies such as doping, a coupling of two or more semiconductors. The coupling of semiconductors forms a heterojunction to reduce the recombination rate of the photogenerated charge carriers in the use of environmental purification and remediation. It can also significantly enhance the optical absorption of photocatalyst ⁹. Among the combinations reported, ZnO has been successfully fabricated combined with Fe₂O₃ ¹⁰, showing in both cases improved properties. Iron oxide due to its narrow bandgap energy and using this to reduce the energy gap between the conduction band and valence band.

Several attempts also have been made to improve the efficiency of photocatalysts by using doping materials. Doping is required to improve the efficiency of photocatalysts. The reduction of the optical energy gap of ZnO by doping is an advantage for use in optoelectronic devices. Among these doping materials, Ag-doped ZnO ¹¹, N-doped ZnO ¹², Mg-doping on ZnO ¹³, Cu-doped iron oxide ¹⁴, nitrogen N-S-co-doped single nanomaterials have been successfully used like TiO₂ ¹⁵. This work confirms the increasing photodegradation efficiency of N/Ag-doped ZnO-Fe₂O₃ nanoparticle photocatalyst by doping it onto the silver and nitrogen. Indeed, N/Ag-doped ZnO-Fe₂O₃ nanoparticles were produced using of solid-state reaction. This favored the improvement of the photocatalytic activity of the doped nanocomposite under irradiation with visible light for the photodegradation of MB.

2. Experimental

2.1. Synthesis of the catalysts

2.1.1. Preparation of ZnO-Fe₂O₃ Nanocomposite

The nanocomposite of ZnO-Fe₂O₃ was prepared by precipitation method using the mixture of solutions of iron (III) nitrate nonahydrate (Fe (NO₃)₃.9H₂O) and zinc nitrate hexahydrate (Zn (NO₃)₂.6H₂O) which were separately prepared. To this mixture, a solution of sodium carbonate (Na₂CO₃) was added for precipitating the binary mixed oxides of ZnO-Fe₂O₃. For this purpose, 4.7 mmol of Zn (NO₃)₂.6H₂O and 0.5 mmol of Fe (NO₃)₃.9H₂O salts were dissolved in 100 mL DI water and mixed in a beaker. To this mixture, a solution of Sodium

carbonate (Na₂CO₃) was added with continuous stirring for 3 h for precipitating the precursors as mixed oxide. The precipitate thus formed by the reaction of the two solutions was left to stand for 24 h. It was then filtered off 0.2 μm membrane filter (Whatman) and washed three times each time with DI water and ethanol. The final precipitate was dried at 100°C for 3 h and calcined at 300°C for 24 h in a programmable furnace to get ZnO-Fe₂O₃ mixed oxides nanoparticles ¹⁶. The product was labeled as ZnO-Fe₂O₃.

2.1.2. Preparation of N-doped ZnO-Fe₂O₃ Nanoparticles

The ZnO-Fe₂O₃ prepared was mixed with urea, with a predetermined urea/ ZnO-Fe₂O₃ molecular ratio (1:3) for a few minutes in agar mortar. The mixture was then transferred to a ceramic crucible and was calcinated at 400°C for four hours for solid-phase reaction ¹⁷. The product obtained was labeled as nitrogen-doped ZnO-Fe₂O₃.

2.1.3. Synthesis of Ag-doped ZnO-Fe₂O₃ Nanocomposite

10 ml of silver nitrate (0.18 M) was added to 10 g of uncalcined ZnO-Fe₂O₃. The sample was agitated and heated at 110°C for 30 minutes. The powder was cooled to room temperature, calcined at 400°C for 4 hrs, and then ground in an agate mortar ¹⁸. The product obtained was labeled as silver-doped ZnO-Fe₂O₃.

2.1.4. Preparation of silver-nitrogen co-doped ZnO-Fe₂O₃ Nanoparticles

10 ml of silver nitrate (0.18 M) was transferred into a ceramic crucible containing 10 g of Nitrogen-doped ZnO-Fe₂O₃ and was agitated with a glass rod. The crucible was put in an oven for drying at 110°C for 30 minutes. The dried powder was calcined at 400°C for 4 hrs, cooled to room temperature, and was ground in an agate mortar. The obtained product was labeled as silver-nitrogen co-doped ZnO-Fe₂O₃. A light source is a light bulb with a tungsten filament(300-2500nm), a deuterium arc lamp, which is continuous over the ultraviolet region (190-400nm) and Zenon arc lamp, which is continuous from 160 to 2000nm.

Table 1. Designation of the ZnO-Fe₂O₃, Ag-doped ZnO-Fe₂O₃, N-doped ZnO-Fe₂O₃, and Ag/N co-doped ZnO-Fe₂O₃ Photocatalysts.

Sample code	Experimental conditions
b1	ZnO-Fe ₂ O ₃
b2	Ag-doped ZnO-Fe ₂ O ₃
b3	N-doped ZnO-Fe ₂ O ₃
b4	Ag/N co-doped ZnO-Fe ₂ O ₃

2.2. Photocatalytic Studies

2.2.1. Photocatalytic degradation studies of Methylene blue

The photocatalytic activity of each material was estimated by measuring the decomposition rate of MB dye aqueous solution under visible light irradiation. The visible light irradiation was carried out by projecting light from a tungsten lamp (40 W, 220 V, 1.8 A, 50 Hz frequency) in a photoreactor. Reaction suspensions were prepared by adding the required amount of photocatalyst into 100 mL of MB solution, taken with different initial dye concentrations. The aqueous suspension containing MB and the photocatalyst was irradiated with constant stirring. The samples were collected at regular intervals of time (20 min), centrifuged, and filtered before measuring the absorbance¹⁹. The photodegradation of MB in each sample was analyzed by using a UV-visible spectrophotometer (SP65) at a wavelength of 460 nm (max of the MB dye), and the percentage degradation of MB was calculated using the relation²⁰.

$$\% \text{ Degradation} = \frac{A_i - A_0}{A_i} \times 100 \quad \text{Eq. 1}$$

Where A_0 is the absorbance of dye at the initial stage, A_t is the absorbance of the dye at the time "t".

In this section, the photocatalytic degradation experiments were carried out in the dark with the presence of each photocatalyst in the presence of radiation and were studied.

3. Results and Discussion

3.1. Characterization of the Catalysts

3.1.1. XRD analysis

Figure 1 depicts the XRD patterns of the synthesized pure ZnO-Fe₂O₃, Ag-doped ZnO-Fe₂O₃, N-doped ZnO-Fe₂O₃, and Ag/N co-doped ZnO-Fe₂O₃ nanocomposite. The diffraction peaks observed at scattering angles $2\theta = 31.87, 34.48, 36.33, 47.52, 56.64, 62.93, 66.52, 68.17, 69.13, 72.63$ and 76.95 represent typical Hexagonal Wurtzite structure of ZnO (b1, b2, b3 and b4). The fact that more of the peaks are represented ZnO is in line with the proportion of the components. ZnO is the major component, and hence the listing crystal more peaks representing ZnO in the diffraction patterns of b1. The prevailing diffraction peaks of ZnO are also apparent in the mixtures (b2, b3, and b4). Almost all the peaks do represent the diffraction peaks of wurtzite ZnO structures. The only peaks representing Fe₂O₃ could be the peaks at 2θ value of 36.33 and 62.88 representing the maghemite phase of Fe₂O₃. The calcination temperature employed, that is, 300°C , is not good enough to bring about enough peaks of either maghemite or hematite.

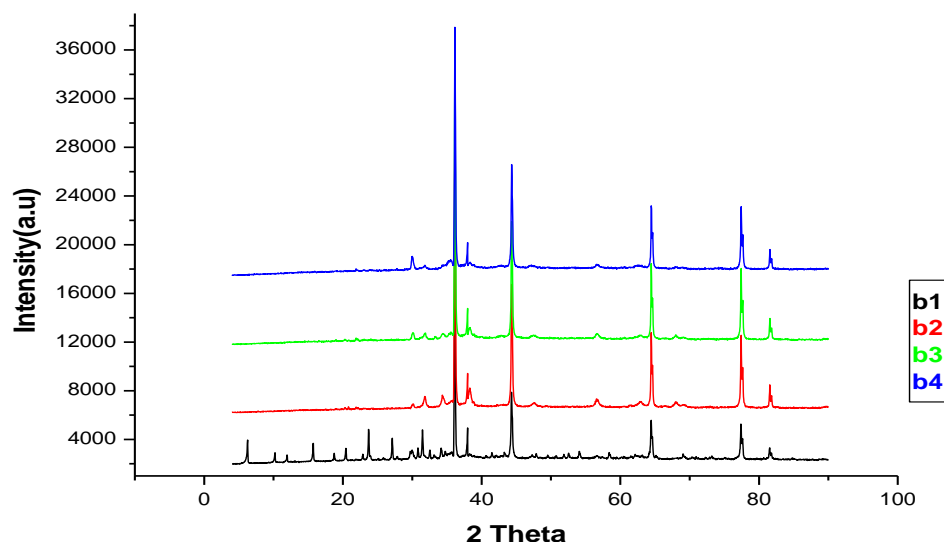


Figure 1. XRD diagram of b1, b2, b3 and b4

The average crystallite size of the as-synthesized nanoparticle (photocatalysts) was obtained using the Debye-Scherrer formula.

$$D = \frac{K\lambda}{\beta \cos\theta} \quad \text{Eq. 2}$$

Where D = crystallite size in nm

K = the shape factor constant and taken as 0.9; β is the full width at half maximum (FWHM) in radians, λ is the wavelength of the X-ray (0.15406 nm) for Cu target $K\alpha_1$ radiation and θ is the Bragg's angle. The calculated average crystalline size of the as-synthesized photocatalysts is recorded in Table 2.

Table 2. Crystal size of ZnO-Fe₂O₃, Ag-doped ZnO-Fe₂O₃, N-doped ZnO-Fe₂O₃ and Ag-N co-doped ZnO-Fe₂O₃ powders.

Nanocomposite	2θ (degree)	β (radians)	D (nm)	Bandgap (E _g) (eV)
b1	36.203	0.0041	35.4	2.74
b2	36.236	0.0046	33.2	2.48
b3	36.136	0.0046	32.15	2.17
b4	36.124	0.0063	24.12	2.04

3.2. Analysis of UV-visible diffuses reflectance absorption spectra of as-synthesized materials

UV-visible diffuse reflectance spectroscopic data of ZnO-Fe₂O₃, Ag-doped ZnO-Fe₂O₃, N-doped ZnO-Fe₂O₃, and Ag/N co-doped ZnO-Fe₂O₃ (b₁, b₂, b₃, b₄ respectively) obtained from the plots of absorbance against wavelength (Figure 2) are discussed as follow. The intercept of the tangent line on the descending part of the absorption peak at the wavelength axis gives the value of reflectance (nm). Estimation of bandgap energy using the above approach sometimes may not provide a clear tangential line when the peak is not well resolved for a given sample. This could probably happen when the scattering effect is as high as the optical absorption processes. In such case, scattering screens the absorption peak, making the assignment of bandgap energy (E_g) uncertain. To avoid difficulties in obtaining the bandgap energy, for example, from UV-visible absorption spectroscopy in scattered samples, diffuse reflectance spectroscopy (DRS) was used. The transformed the data obtained from UV-visible diffuse reflectance spectroscopy to suppress the bandgap estimation obtained from a plot of absorbance against wavelength using the equation below²¹.

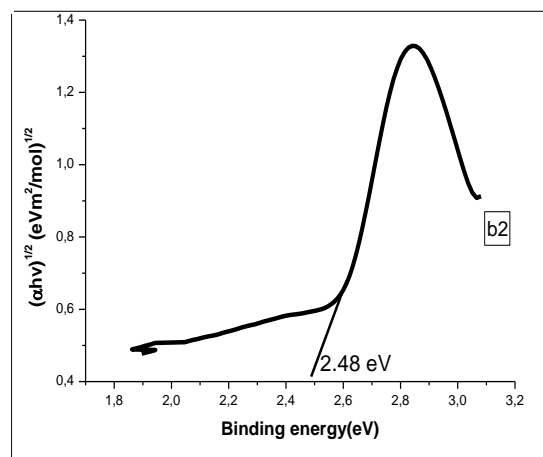
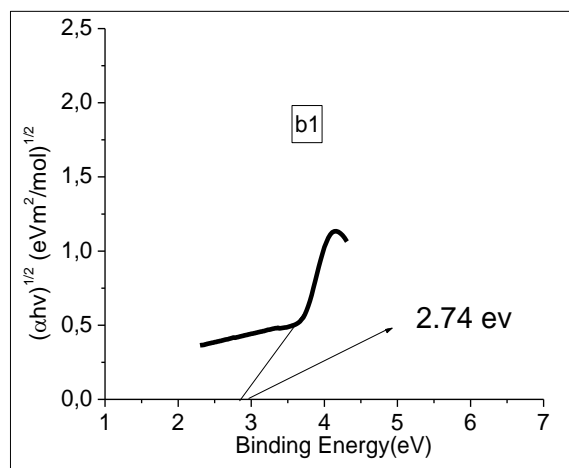
$$\alpha h\nu = A (h\nu - E_g)^{n/2} \quad \text{Eq. 3}$$

Where α , $h\nu$, A , and E_g are optical absorption coefficient, the photonic energy, proportionality constant, and bandgap, respectively. In this equation, n decides the type of the transition in a

semiconductor ($n=1$, direct absorption; $n=4$, indirect absorption). By applying $n=1$, the direct bandgap of the prepared photocatalyst was determined from the plot of $(\alpha h\nu)^{1/2}$ vs. $h\nu$, as indicated in the inset of Figure 2. Accordingly, the estimated bandgaps by extrapolating the straight line to the x-axis for ZnO-Fe₂O₃¹³, Ag-doped ZnO-Fe₂O₃, N-doped ZnO-Fe₂O₃ and Ag-N co-doped ZnO-Fe₂O₃ (b₁, b₂, b₃, b₄) were found to be 2.74, 2.48, 2.17 and 2.05 eV respectively.

The results indicated that nanocomposite photocatalysts exhibit a redshift which widens the absorption wavelength and allows the composite to absorb in the visible region due to their lower bandgaps. These all happen due to the coupling of Fe₂O₃ with ZnO^{12,13}, Ag-doped ZnO-Fe₂O₃, N-doped ZnO-Fe₂O₃, and Ag/N co-doped ZnO-Fe₂O₃, and Ag/N co-doped ZnO-Fe₂O₃ is the dominant factor in decreasing the bandgap due to co-doping Ag and N.

The reflectance property is a crucial factor to consider when selecting a photocatalyst. Figure 2 shows the UV-vis reflectance spectra of ZnO-Fe₂O₃, Ag-doped ZnO-Fe₂O₃, N-doped ZnO-Fe₂O₃, and Ag-N co-doped ZnO-Fe₂O₃ (b₁, b₂, b₃, b₄). It can be seen that the Ag/N co-doped ZnO-Fe₂O₃ compared with the Ag-doped ZnO-Fe₂O₃ and N-doped ZnO-Fe₂O₃, the absorption intensity slightly increases. This result indicates that Ag/N co-doped ZnO-Fe₂O₃ is a potential photocatalyst for sunlight-driven applications.



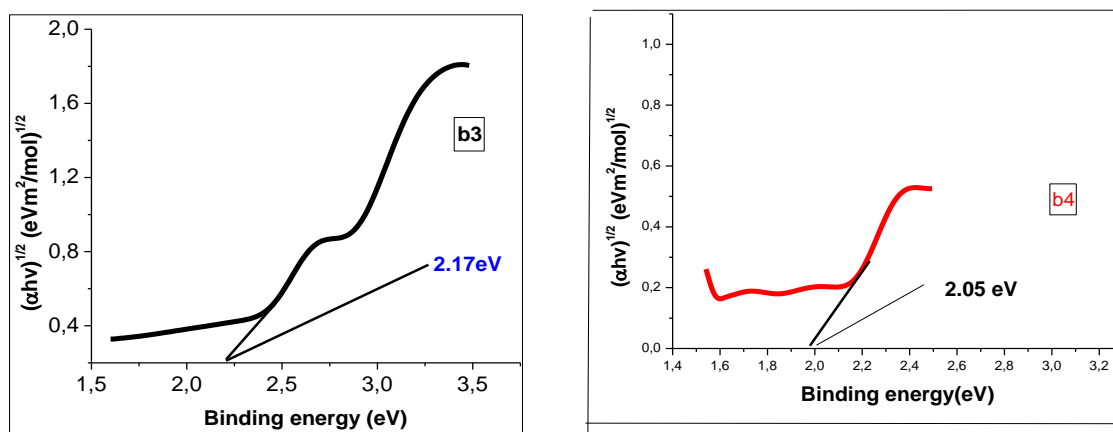


Figure 2. UV-visible diffuse reflectance of b₁, b₂, b₃, and b₄

3.3. Photocatalytic Studies

3.3.1. Comparison of photocatalytic activities of the as-synthesized photocatalysts

The photocatalytic activities of ZnO-Fe₂O₃, Ag-doped ZnO-Fe₂O₃, N-doped ZnO-Fe₂O₃, and Ag/N co-doped ZnO-Fe₂O₃ using initial dye concentrations of 10 mg/L and with 110 mg/L photocatalyst load were evaluated under visible light. The highest % degradation of the photocatalysts b₁, b₂, b₃ & b₄, was 45.11, 47, 51, and 64.5. As indicated in Figure 3, the results reveal that the smallest degradation efficiencies of b₁ and b₂ are due to their large bandgaps.

The photocatalytic activity of Ag/N co-doped ZnO-Fe₂O₃ nanocomposite was higher than all the as-synthesized photocatalysts: b₁, b₂, and b₃, this is due to co-doping of Ag-N in the composite.

In general, the photocatalytic activities of b₁ < b₂ < b₃ < b₄ under irradiation with visible light and the highest percentage of photocatalytic degradation were 64.5%, which is for b₄ and it was selected for the following experiments.

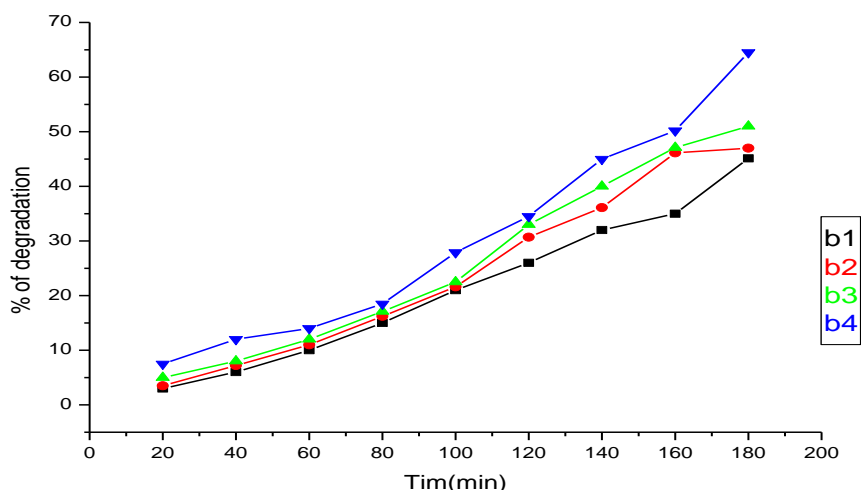


Figure 3. Plots of % degradation of Methylene blue as a function of time under visible irradiation using b₁, b₂, b₃ and b₄ photocatalysts: Methylene blue = 10 mg/L, catalyst load = 110 mg/L

3.3.2. Effect of the solution pH

To study pH effect on catalytic efficiency of b₄, experiments were conducted at pH 2, 3, 5, 6, 8, 10, and 12. The Methylene blue % degradation at pH 2, 3, 5, 6, 8, 10 and 12 were 40.1, 43.53, 55.1, 67, 62, 57 and 54, respectively. These results show that the Methylene blue degradation efficiency was increased from 40.1 to 67 from pH 2 to pH 6 and decreased from 62, 57 to 54 from pH 8 to 12 in 180 min as

indicated in Figure 4. These may be due to the less availability of OH⁻ ions to form highly active OH⁻ radicals. Beyond pH 7 (for higher pH), the catalyst surface becomes negatively charged and causes electrostatic repulsion between the catalyst and negatively charged Methylene blue. As a result, degradation efficiency decreased. Since the photodegradation was most effective at pH 6, the subsequent experiments were continued at pH 6.

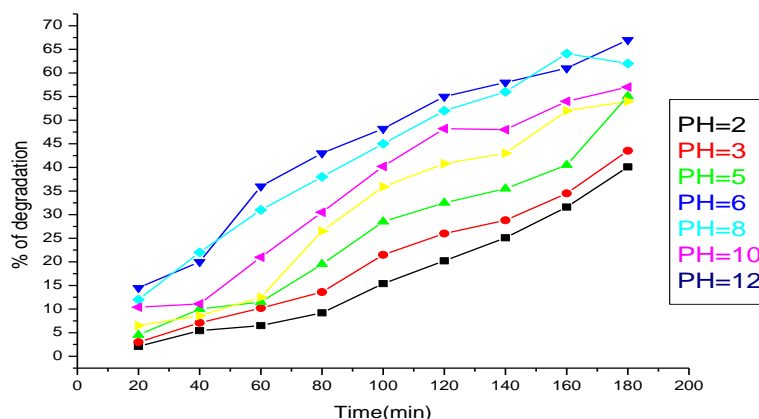


Figure 4. Plots of % degradation of Methylene blue as function of time under visible irradiation using b_4 photocatalyst: Methylene blue = 5 mg/L, catalyst load=110 mg/L, pH 2-12

3.3.3. Study of Point of Zero Charge (PZC) of Ag/N co-doped ZnO-Fe₂O₃

The PZC is a point at which the surface charge of the photocatalyst is zero or neutral that lies in the pH range of 4.5 - 7.0, depending on the catalysts used. Due to the absence of an electrostatic force between photocatalyst and dye particles, the interaction (adsorption) and photocatalysis processes are very less at PZC. When the pH of the system under study is higher than the PZC, the photocatalyst surface will be negatively charged, and the repulsion between the photocatalyst and cationic (MB) at pH greater than the PZC, interaction and photocatalysis is higher. Still, at pH, less than the PZC of the photocatalyst, the repulsion is higher, and the photocatalysis is lesser²⁰.

As illustrated in Figure 5 the point of zero charge of Ag/N co-doped ZnO-Fe₂O₃ was investigated between pH of 2.0 and 12.0. The PZC of the photocatalyst was found to be 6.52, which is expected to be the point at which the surface charge of the synthesized photocatalyst is neutral. The above photodegradation result revealed that higher adsorption and higher photocatalysis were obtained at pH less than the PZC of the catalyst, which is pH = 5.0. This is due to the higher interaction between the positively charged surface of the photocatalyst particles and the negatively charged MB molecules at this pH. At a pH = 1.0, complete bleaching (decolorizing) of the photocatalyst was observed.

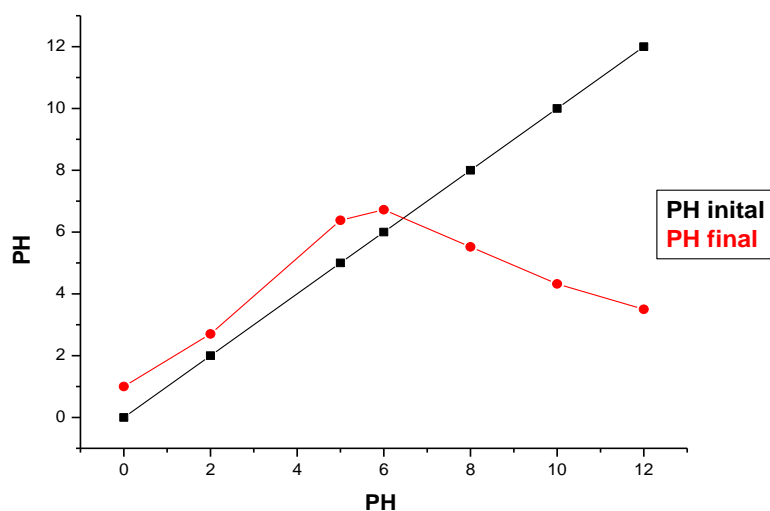


Figure 5. Plot of Point of Zero Charge of Ag/N co-doped ZnO-Fe₂O₃ photocatalyst

3.3.4. Effect of initial dye concentration

The effect of the initial substrate concentration on the degradation of Methylene blue was studied using different concentrations of the dye 5, 10, 15, 20, and 25 mg/L by keeping the photocatalyst load 110 mg/L and at pH 6. The highest recorded percentage degradation of Methylene blue at these concentrations was 77, 74.1, 70.13, 64.12, and 54.3, respectively. From the above results, the highest

degradation was found to be maximum at 5 mg/L initial concentration of Methylene blue, as indicated in Figure 6. The photodegradation rate decreases when dye concentration increases. It is because, at a higher concentration of dye, the number of interacting radiation photons per dye molecule decreases²³. Further, at more top dye initial concentration, the approach of the radiation photons to the catalyst surface is hindered and screened off,

thereby, reducing the photocatalytic activity in the system²⁴. Moreover, at the higher dye concentration, the number of collisions between dye molecules

increases at the cost of required collisions between dye molecules and OH radical. Therefore, the rate of reaction is retarded²⁵.

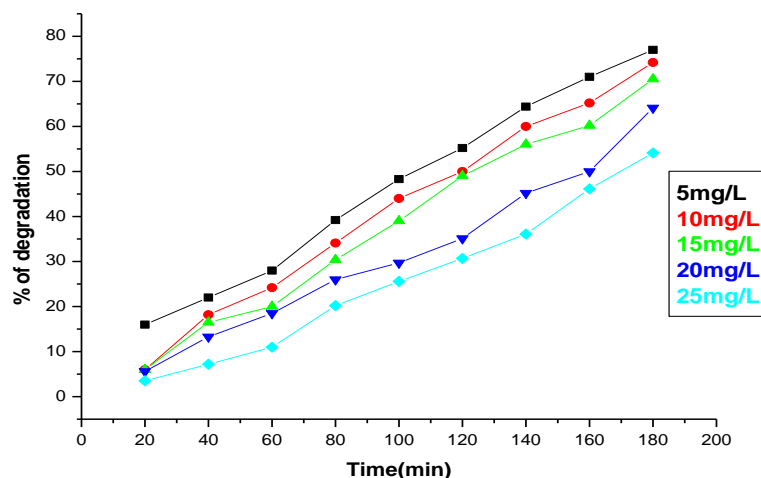


Figure 6. Plots of % degradation of Methylene blue as a function of time under visible light irradiation by keeping the b_4 photocatalyst load constant and varying the amount of MB solution

3.3.5. Effect of photocatalyst load

The MB degradation efficiency using different catalyst concentrations of 30, 50, 70, 90, and 110 mg/L were studied with an initial dye concentration of 5 mg/L at pH=6 within 180 min. The highest % degradations for the given concentrations were 60, 65, 71, 78, and 74, respectively, as indicated in Figure 7. This is a meaningful way to check out and select one with an optimum photocatalyst concentration for avoiding excess photocatalyst and ensuring total adsorption of energetic photons²⁵. Thus, this induces catalyst aggregation where the catalyst becomes larger, leading to catalyst sedimentation²⁶. This is because an unfavorable light scattering and reduction of light penetration into the solution is observed with excess photocatalyst loading. From the above results, 78 %

was the highest % degradation by b_4 for the 90 mg/L in 180 min. The remaining dosages' degradation efficiency was less, and at 110 mg/L, it was recorded 60% in 180 min. The increase of the photocatalytic efficiency seems to be due to the rise in the total surface area available for the photocatalytic reaction as the loading of photocatalyst increased. However, the photodegradation efficiency of b_4 photocatalyst was decreased beyond 90 mg/L (catalyst concentration). Then the number of active sites on the b_4 surface may become almost constant because of the reduced light penetration via shielding effect of the suspended particles²⁷ and the loss in the surface area caused by agglomeration²⁸. Therefore, 90 mg/L of the photocatalyst was selected as the optimal amount of photocatalyst for the subsequent experiments, since it was the most effective²⁹.

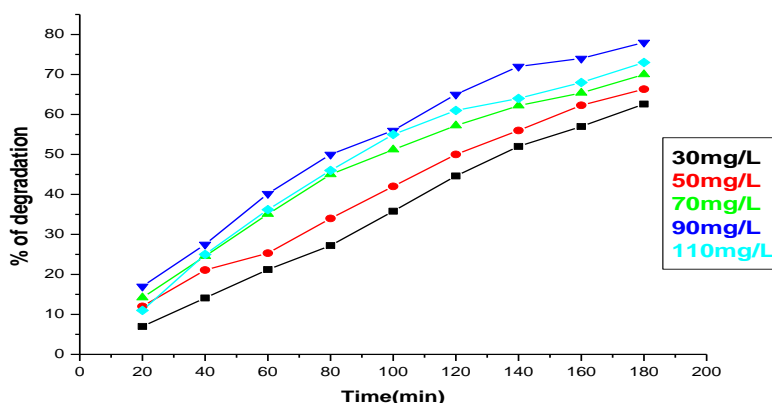


Figure 7. Plots of % degradation of Methylene blue as a function of time under visible light irradiation by varying the b_4 photocatalyst load and keeping the concentration of MB constant

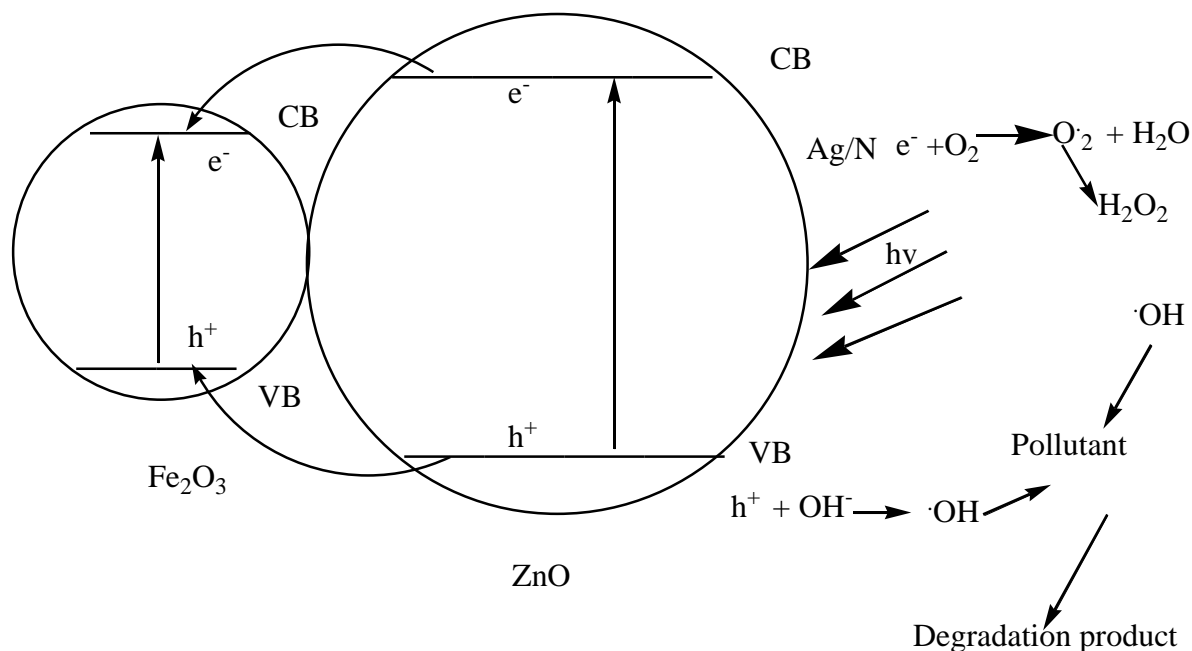


Fig. 8. Proposed mechanism for Ag/N co-doped ZnO-Fe₂O₃ nanocatalyst on the photocatalytic decolorization of Methylene blue under light radiation

4. Conclusions

In conclusion, the optical, structural, and photocatalytic properties of silver and nitrogen co-doped ZnO-Fe₂O₃ nanoparticles were checked. XRD analysis showed that the samples were in the hexagonal-wurtzite phase. Optical absorption measurements indicated a redshift in the edge of the absorption band by doping with silver and nitrogen. This study suggested that silver and nitrogen doping reduced energy deficit. The photocatalytic activity of the ZnO nanoparticles was improved by Ag and N doping. Also, the decolorization efficiency of Methylene blue depended on the amount of silver and nitrogen.

Acknowledgments

The author thanks the staff of the department of chemistry, college of natural and computational sciences in Mizan-Tepi University for assisting with this research

References

- 1- G. Crini, Non-conventional low-cost adsorbents for dye removal: A review, *Bioresour. Technol.*, **2006**, 97, 1061–1085.
- 2- D. I. Petkowicz, R. Brambilla, C. Radtke, C. D. S. da Silva, Z. N. da Rocha, S. B. C. Pergher, J. H. Z. dos Santos, Photodegradation of methylene blue by in situ generated titania supported on a NaA zeolite, *Appl. Catal: A*, **2009**, 357, 125–134.
- 3- U. I. Gaya, A. H. Abdullah, Heterogeneous photocatalytic degradation of organic contaminants over titanium oxide: A review of fundamentals, progress, and problems, *J. Photochem. Photobiol C.*, **2008**, 9, 1-12.
- 4- J. M. Herrman, Heterogeneous photocatalysis: fundamentals and applications to the removal of various types of aqueous pollutants, *Catalysis Today*, **1999**, 53, 115-129.
- 5- C. Shifu, Z. Wei, Z. Sujuan, L. Wei, Preparation, characterization, and photocatalytic activity of N-containing ZnO powder, *Chem. Eng. J.*, **2009**, 148, 263–269.
- 6- D. Chatterjee, D. Shimanti, A novel visible-light-driven photocatalyst film, MoS₂/Ag/TiO₂, was synthesized on a glass-fiber, *Photochem. Rev.*, **2005**, 6, 186-205.
- 7- S. Sakthivel, M. Janczarek, H. Kisch, Visible light activity and photoelectrochemical properties of nitrogen-doped TiO₂, *J. Phys. Chem.*, **2004**, 108, 19384-19387.
- 8- M. Pera-Titus, V. Garcia-Molina, M. Bˆanos, J. Gimˆenez, S. Esplugas, *Appl. Catal B- Environ.*, **2004**, 47, 219-256.
- 9- G. Yang, Z. Yan, T. Xiao, Preparation and characterization of SnO₂/ZnO/TiO₂ composite semiconductor with enhanced photocatalytic activity, *Appl. Surf. Sci.*, **2012**, 258, 8704–8712.
- 10- D. Sarkar, G. G. Khan, A. K. Singh, K. Mandal, Enhanced electrical, optical, and magnetic properties in multifunctional ZnO-Fe₂O₃ semiconductor nano-heterostructures by heterojunction engineering, *J. Phys. Chem. C.*, **2012**, 116, 23540–23546.
- 11- S. G. Shelar, V. K. Mahajan, G. H. Sonawane, Effect of doping parameters on photocatalytic degradation of methylene blue using Ag-doped ZnO nanocatalyst, *SN Applied Sciences*, **2020**, 2, 1-10.
- 12- M. Zheng, J. Wu, One-step synthesis of nitrogen-doped ZnO nanocrystallites and their properties, *Appl. Sur. Sci.*, **2009**, 255, 5656–5661.

- 13-K. Pradeev raj, K. Sadaiyandi, A. Kennedy, S. Sagadevan, Z. Z. Chowdhury, M. R. B. Johan, F. Abdul Aziz, F. R. Rafique, R. T. Selvi, R. R. bala, Influence of Mg Doping on ZnO Nanoparticles for Enhanced Photocatalytic Evaluation and Antibacterial, **2018**, 13, 229.
- 14-I. Fernández-Barahona, L. Gutiérrez, S. Veintemillas-Verdaguer, J. Pellico, M. del Puerto Morales, M. Catala, M. A. del Pozo, J. Ruiz-Cabello, F. Herran, Cu-Doped Extremely Small Iron Oxide Nanoparticles with Large Longitudinal Relaxivity: One-Pot Synthesis and in Vivo Targeted Molecular Imaging, ACS omega, **2019**, 4, 2719–2727.
- 15-F. Wei, L. Ni, P. Cui, Preparation and characterization of N–S-codoped TiO₂ photocatalyst and its photocatalytic activity., J. Hazard. Mater., **2008**, 156, 135–140.
- 16-M. L. Maya-Treviño, J. L. Guzmán-Mara, L. Hinojosa-Reyes, N. A. Ramos-Delgado, M. I. Maldonado, A. Hernández-Ramírez, Activity of the ZnO–Fe₂O₃ catalyst on the degradation of dicamba and 2,4-D herbicides using simulated solar light, *Ceram. Int.*, **2014**, 40, 8701–8708.
- 17-Y. Huang, X. Zheng, Y. Zhongyi, T. Feng, F. Beibei, H. Keshan, Preparation of Nitrogen-doped TiO₂ Nanoparticle Catalyst and Its Catalytic Activity under Visible Light, *Inter. J. of Photoenergy*, **2007**, 802-807.
- 18-V. Mirkhani, S. Tangestaninejad, M. Moghadam, Photocatalytic degradation of azo dyes catalyzed by Ag-doped TiO₂ photocatalyst, *J Iran Chem Soc.*, **2009**, 6, 578–587.
- 19-R. Saravanan, H. Shankar, T. Prakash, V. Narayanan, A. Stephen, ZnO/CdO composite nanorods for photocatalytic degradation of methylene blue under visible light, *Mater. Chem. Phys.*, **2011**, 125, 277–280.
- 20-J. Zhang, K. Yu, L. Lou, C. Ma, L. Liao, M. Yi, S. Liu, Visible-Light Photocatalytic Activity of 21-Ag₃PO₄ with Different Particle Sizes for the Degradation of Bisphenol A in Water, *Disaster Adv.*, **2013**, 6, 109-117.
- 22-J. Cao, B. D. Luo, B. Xu, S. Chen, Aluminum salt sludge characterization and utilization. A review article, *Journal of Hazardous Materials*, **2012**, 217, 1-10.
- 23-Mark Kosmulski, “Chemical Properties of Material Surface” Marcel Dekker Inc, New York, Basel, 2001.
- 24-R. J. Davis, J. L. Gainer, G. O. Neal, I. W. Wu, Photocatalytic Decolorization of Wastewater Dyes, *Water Environ. Res.*, **1994**, 66, 50–53.
- 25-G. A. Epling, C. Lin, Photo assisted bleaching of dyes utilizing TiO₂ and visible light, *26-Chemosphere*, **2002**, 46, 561-570.
- 27-S. Lodha, D.Vaya, R. Ameta, P. Punjabi,
- 28-Photocatalytic degradation of Phenol Red using complexes of some transition metal and hydrogen peroxide, *Journal Chemical Society.*, **2008**, 73, 631-63.
- 29-M. Qamar, M. Muneer, Comparative photocatalytic study of two selected pesticide derivatives, indole-3-acetic acid, and indole-3-butyric acid in aqueous suspensions of titanium, *Journal of Hazardous Materials*, **2005**, 120, 219-227.
- 30-A. Burns, W. Li, C. Baker, S. I. Shah, Sol-gel synthesis and characterization of neodymium-ion doped nanostructured titania thin film. *Mater. Journal of material science*, **2001**, 703, 193–198.
- 31-X. Chen, S. S. Mao, Titanium dioxide nonmaterial: synthesis, properties, modifications, and applications, *Chemical Reviews*, **2007**, 107, 2891–2959.
- 32-D. W. Bahnemann, Mechanisms of organic transformations on semiconductor particles, *Photochemical Conversion and Storage of Solar Energy*, **1991**, 251-276.